Numerical analysis of embankment primary consolidation with porosity-dependent and strain-dependent coefficient of permeability

Anis Balic[a], Emina Hadzalic* and Samir Dolarevic[b]

*Faculty of Civil Engineering, University of Sarajevo, Patriotske lige 30, 71000 Sarajevo,
Bosnia and Herzegovina*

Abstract. The total embankment settlement consists of three stages: the initial settlement, the primary consolidation settlement, and the secondary consolidation settlement. The total embankment settlement is largely controlled by the primary consolidation settlement, which is usually computed with numerical models that implement Biot's theory of consolidation. The key parameter that affects the primary consolidation time is the coefficient of permeability. Due to the complex stress and strain states in the foundation soil under the embankment, to be able to predict the consolidation time more precisely, aside from porosity-dependency, the strain-dependency of the coefficient of permeability should be also taken into account in numerical analyses. In this paper, we propose a two-dimensional plane strain numerical model of embankment primary consolidation, which implements Biot's theory of consolidation with both porosity-dependent and strain-dependent coefficient of permeability. We perform several numerical simulations. First, we demonstrate the influence of the strain-dependent coefficient of permeability on the computed results. Next, we validate our numerical model by comparing computed results against in-situ measurements for two road embankments: one near the city of Saga, and the other near the city of Boston. Finally, we give our concluding remarks.

Keywords: embankment; permeability; porosity-dependency; primary consolidation; settlement; strain-dependency

1. Introduction

The main challenge in the design of highway and road embankments is in predicting the construction time. Namely, the works on the pavement structure can commence after the design-determined embankment settlement has occurred. This design-determined value of the embankment settlement is smaller than the predicted total value of the settlement and is obtained by subtracting the allowed value of the settlement that can occur during and after the construction of the pavement structure from the predicted total value of the embankment settlement. Thus, in order to determine the time at which the works on the pavement structure can begin, the total embankment settlement has to be computed.

*Corresponding author, Assistant Professor, E-mail: emina.hadzalic@gf.unsa.ba
[a]Assistant Professor, E-mail: anis.balic@gf.unsa.ba
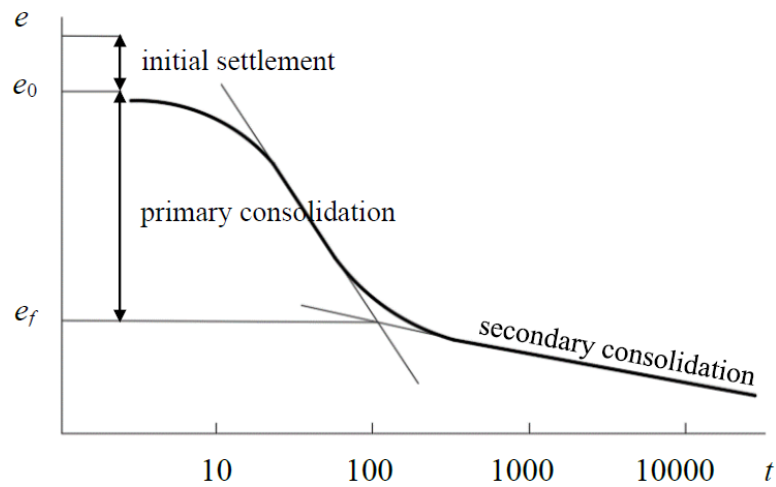[b]Professor, E-mail: samir.dolarevic@gf.unsa.ba

Fig. 1 Three stages of embankment total settlement (Maksimović 2008)

The total settlement of embankment on soft soil can be divided into three stages (Fig. 1) (Maksimović 2008). The first stage is the elastic or immediate settlement, which occurs immediately after the load is applied. This part of the total settlement is due to the deformation of the soil in undrained conditions where there is no change in the soil volume and in the soil water content. The immediate settlement can be computed by using a linear elastic model with linear elastic parameters that correspond to undrained conditions (Chin 2005). The immediate settlement can be challenging to determine since it is dependent on the rate of embankment construction. In the embankment design, it is often assumed that the initial settlement is of the order of 10-20% of the primary consolidation settlement of the embankment.

The primary consolidation settlement is the second stage, which starts after the soil has settled elastically. The primary consolidation settlement is due to the compression of the soil skeleton as a result of the expulsion of the water from the pores under the applied load. Namely, the load applied to the saturated soil is first carried by the water in the pores, which causes a rise in pore water pressures, called excess pore pressures. The excess pore pressures build-up causes the water to drain out of the pores. Due to the expulsion of the water from pores, the load is gradually transferred from the pore water to the soil skeleton. This results in a decrease of the pore water pressures and in an increase in the effective stresses. The change in effective stresses causes the compression of the soil skeleton, resulting in a decrease in the soil volume, i.e., the settlements. The excess pore pressures dissipate over time as the water flows out from the pores. The consolidation is considered to end after the excess pore pressures drop to zero, since there is no more change in effective stresses, hence neither in the soil volume. The end result of the primary consolidation analysis is the consolidation curve, which provides two key information: the consolidation magnitude and the time rate of consolidation. i.e., the consolidation time. The primary consolidation analysis usually relies on Terzaghi's theory of one-dimensional consolidation (Terzaghi 1943) and Biot's theory of three-dimensional consolidation (Biot 1941). Both theories assume that the soil is linear elastic, deformations are small, and the pore water flow is governed by Darcy's law. Furthermore, the compressibility and the permeability of the soil are assumed constant during the consolidation process. Other methods, such as Asaoka's method or hyperbolic method, are also used (Li 2014, Radhika *et al*. 2020).
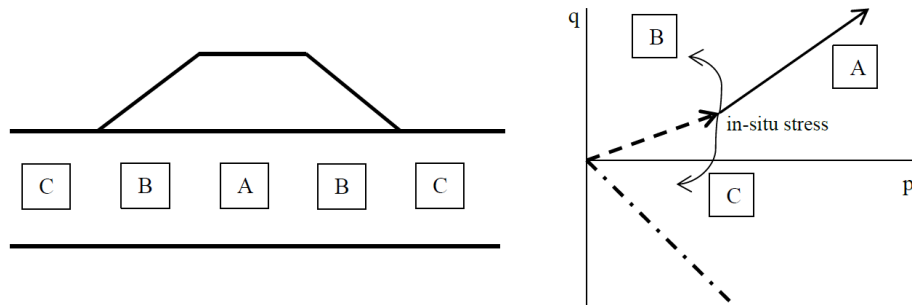
Fig. 2 Zones in soil under the embankment with different strain states

The third stage is the secondary consolidation settlement (or secondary compression), which is due to the rearrangement of soil particles (Chin 2005). The secondary consolidation settlement is assumed to start after the completion of 90% of primary consolidation settlement since it takes infinite time for complete primary consolidation settlement to occur. The secondary consolidation settlement mainly depends on the coefficient of secondary compression C_α.

The primary consolidation settlement influences the most the total embankment settlement. For computing the primary consolidation magnitude and consolidation time, numerical models that implement Biot's theory of consolidation are commonly used (Huang 2006, Al-Shakarchi *et al.* 2009, Singh and Sawant 2014, Tasiopoulou *et al.* 2015a, 2015b, Müthing *et al.* 2018, Hadzalic *et al.* 2018, 2020). The consolidation magnitude is controlled by the deformability parameters of the soil, and the consolidation time by the permeability parameters expressed through the coefficient of permeability. The porosity-dependence of the coefficient of permeability is commonly assumed in numerical analyses and is implemented in various geotechnical software, such as Plaxis (Di and Sato 2003, Xie and Leo 2004, Zhuang *et al.* 2005, Geng *et al.* 2006, Zou *et al.* 2017, Plaxis 3D Reference Manual, 2021). However, various authors suggest that the coefficient of permeability should also be taken as strain-dependent consolidation (Rowe 1959, Kirby and Blunden 1991, Wong and Li 2001) since the strain and stress states vary in different areas of the soil under the embankment (Fig. 2) (Wood 2009). Namely, in the narrow central area of the soil under the embankment, the lateral movements of the soil are restrained (Fig. 2, zone A). However, in other areas (Fig. 2, zones B and C), the deformation occurs in both horizontal and vertical directions. This suggests that, in order to be able to more precisely compute the consolidation time, the coefficient of permeability should be taken as strain-dependent. The strain-dependent coefficient of permeability is proposed in (Balic 2018, Balic *et al.* 2021), and is validated with experimental and numerical results.

In this paper, we propose a two-dimensional plane strain numerical model of embankment primary consolidation that implements Biot's theory of consolidation with porosity-dependent and strain-dependent coefficient of permeability (Balic *et al.* 2021). First, on the numerical example of a 5 m high embankment resting on clay, we show the influence of the strain-dependent coefficient of permeability on the shape of the consolidation curve. Next, we validate the proposed model by comparing the numerically obtained results against in-situ measurements of primary consolidation settlements of two embankments; one near the city of Saga and the other near the city of Boston.

The outline of the paper is as follows. In Section 2, we present the main details of the finite element formulation of the two-dimensional plane strain numerical model of embankment consolidation. In Section 3, we perform several numerical simulations. We present and discuss the computed results. In Section 4, we give our concluding remarks.

2. Numerical model

The proposed two-dimensional plane strain numerical model of the embankment primary consolidation implements Biot's theory of consolidation (Lewis and Schrefler 1998, Smith and Griffiths 2004, Zienkiewicz and Taylor 2005), with porosity-dependent and strain-dependent coefficient of permeability (Balic 2018, Balic *et al.* 2021). The basic assumptions of the model are that the soil is saturated and linear elastic, the deformations are small, the pore water and soil particles are incompressible, and the pore water flow is governed by Darcy's law.

The governing equations of the model are the equilibrium equation and the continuity equation. The equilibrium equation relies on the Terzhagi's principle of effective stresses, which states that the total normal stress σ is equal to the sum of the effective stress σ' carried by the soil skeleton and the pore pressure p carried by the water in the pores, written as

$$\sigma = \sigma' + bp \tag{1}$$

where b is the Biot coefficient; if the soil particles and the water in the pores are assumed to be incompressible, then $b=1$. The effective part of the total normal stress is computed from the constitutive equations.

The strong form of the equilibrium equation is written as

$$\frac{\partial \sigma'_x}{\partial x} + \frac{\partial \tau_{xy}}{\partial y} + \frac{\partial p}{\partial x} = 0$$
$$\frac{\partial \tau_{xy}}{\partial x} + \frac{\partial \sigma'_y}{\partial y} + \frac{\partial p}{\partial y} = 0 \tag{2}$$

where σ_x' and σ_y' are the effective normal stresses in x and y directions, and τ_{xy} is the shear stress.

The constitutive equations for the linear elastic behavior of soil are written as

$$\sigma'_x = (\lambda + 2\mu)\varepsilon_x + \lambda\varepsilon_y$$
$$\sigma'_y = \lambda\varepsilon_x + (\lambda + 2\mu)\varepsilon_y$$
$$\tau_{xy} = \mu\gamma_{xy} \tag{3}$$

where ε_x and ε_y are strains in x and y directions, γ_{xy} is the shear strain, and λ and μ are Lame's coefficients. The strains are given as

$$\varepsilon_x = \frac{\partial u}{\partial x}; \quad \varepsilon_x = \frac{\partial v}{\partial y}; \quad \gamma_{xy} = \frac{\partial u}{\partial y} + \frac{\partial v}{\partial x} \tag{4}$$

where u and v are displacements in x and y directions.

The strong form of the continuity equation is written as

$$\frac{\partial}{\partial t}\left(\frac{\partial u}{\partial x} + \frac{\partial v}{\partial y}\right) - \frac{k_x}{\gamma_w}\frac{\partial^2 p}{\partial x^2} - \frac{k_y}{\gamma_w}\frac{\partial^2 p}{\partial y^2} = 0 \tag{5}$$

where k_x and k_y are the coefficients of permeability in x and y directions, and γ_w is the unit weight of the water.

The coefficient of permeability is assumed to be both porosity-dependent and strain-dependent. The initial value of the coefficient of permeability k_0 can be obtained directly from the constant head or falling head permeability tests, or indirectly from the standard oedometer test. In the standard oedometer test, the deformation occurs only in the vertical direction since the lateral movements of the soil sample are prevented. The vertical load is applied, and the settlements of the soil sample in time are monitored. In the foundation soil under the embankment, the strain state differs from the case of the standard oedometer test, because deformation occurs in both horizontal and vertical directions. Thus, in order to establish the strain-dependence of coefficient of permeability the numerical model of modified oedometer test, which allows free lateral movement is introduced in (Balic *et al.* 2021). Based on the numerical and experimental results of modified oedometer tests on clay samples, the following expression for strain-dependent coefficient of permeability is proposed in (Balic *et al.* 2021), written as

$$k = \alpha \cdot \frac{\varepsilon_s / \varepsilon_v}{0.66} \cdot k_0 \cdot 10^{\frac{e_0 - e}{c_k}} \tag{6}$$

where ε_v is the volumetric deformation, ε_s is the shear deformation, α is the coefficient of the change in permeability, 0.66 is the ratio of the shear and volumetric deformation in standard oedometer test, e_0 is the initial void ratio of the clay sample, e is the void ratio of clay sample in time and c_k is the constant (0.4-0.5) e_0. The volumetric deformation ε_v and the shear deformation ε_s, are computed as

$$\varepsilon_v = \varepsilon_1 + \varepsilon_2; \quad \varepsilon_s = \varepsilon_1 - \varepsilon_2 \tag{7}$$

The porosity-dependence of the coefficient of permeability in Eq. (6) is adopted from Plaxis (Plaxis 3D Reference Manual 2021).

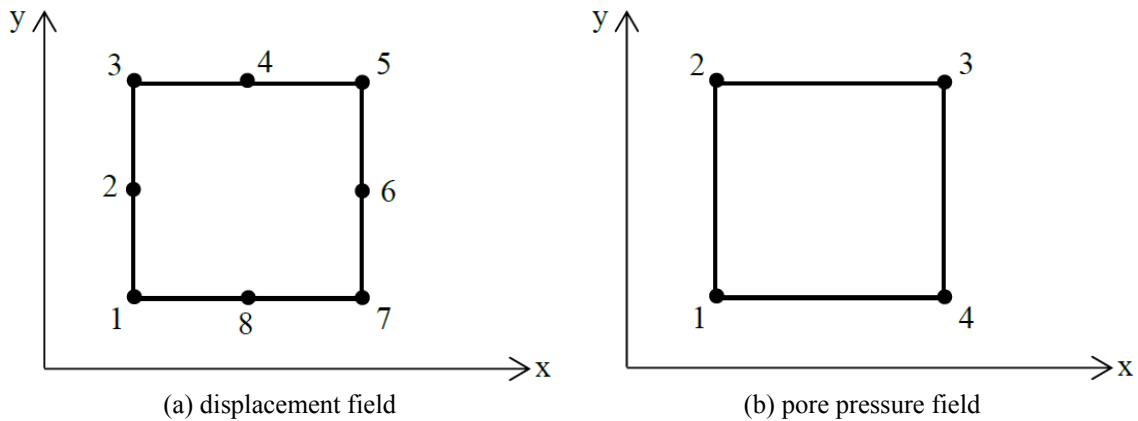(a) displacement field   (b) pore pressure field
Fig. 3 Finite element approximations of unknown fields

Following the standard finite element discretization procedure, we introduce finite element approximations of the displacement and pore pressure fields. Here, we choose **Q8-P4** finite element (Fig. 3), which provides quadratic interpolation of the displacement field and linear interpolation of the pore pressure field. This type of element is shown to be robust for use in coupled problems, such as internal solid phase-pore fluid interaction (Zienkiewicz and Taylor 2005, Ibrahimbegovic 2009).

The end result of the finite element approximation discretization is the following global system of equations, written as

$$\mathbf{K}_m\mathbf{u} + \mathbf{Cp} = \mathbf{f}$$
$$\mathbf{C}^T\dot{\mathbf{u}} - \mathbf{K}_c\mathbf{p} = \mathbf{0}$$

(8)

where $\mathbf{K}_m$ is the stiffness matrix, $\mathbf{K}_c$ is the permeability matrix, $\mathbf{C}$ is the coupling matrix, $\mathbf{f}$ is the external load vector, $\mathbf{u}$ is the vector of unknown nodal displacements, $\dot{\mathbf{u}}$ is the vector of time derivatives of nodal displacements, and $\mathbf{p}$ is the vector of unknown nodal pore pressures. The stiffness matrix $\mathbf{K}_m$, the permeability matrix $\mathbf{K}_c$, and the coupling matrix $\mathbf{C}$ are written as

$$\mathbf{K}_m = \iint \mathbf{B}^T\mathbf{DB}dxdy; \quad \mathbf{K}_c = \iint \mathbf{T}^T\mathbf{kT}dxdy; \quad \mathbf{C} = \iint \mathbf{MN}^P dxdy$$

(9)

where

$$\mathbf{D} = \begin{bmatrix} \lambda + 2\mu & \lambda & 0 \\ \lambda & \lambda + 2\mu & 0 \\ 0 & 0 & \mu \end{bmatrix}; \quad \mathbf{k} = \begin{bmatrix} \dfrac{k_x}{\gamma_w} & 0 \\ 0 & \dfrac{k_y}{\gamma_w} \end{bmatrix};$$

$$\mathbf{B} = \begin{bmatrix} \dfrac{\partial N_1^u}{\partial x} & 0 & \dots & \dfrac{\partial N_i^u}{\partial x} & 0 & \dots & \dfrac{\partial N_8^u}{\partial x} & 0 \\ 0 & \dfrac{\partial N_1^u}{\partial y} & \dots & 0 & \dfrac{\partial N_i^u}{\partial y} & \dots & 0 & \dfrac{\partial N_8^u}{\partial y} \\ \dfrac{\partial N_1^u}{\partial y} & \dfrac{\partial N_1^u}{\partial x} & \dots & \dfrac{\partial N_i^u}{\partial y} & \dfrac{\partial N_i^u}{\partial x} & \dots & \dfrac{\partial N_8^u}{\partial y} & \dfrac{\partial N_8^u}{\partial x} \end{bmatrix}; \quad \mathbf{T}^T = \begin{bmatrix} \dfrac{\partial N_1^P}{\partial x} & \dfrac{\partial N_1^P}{\partial y} \\ \dfrac{\partial N_2^P}{\partial x} & \dfrac{\partial N_2^P}{\partial y} \\ \dfrac{\partial N_3^P}{\partial x} & \dfrac{\partial N_3^P}{\partial y} \\ \dfrac{\partial N_4^P}{\partial x} & \dfrac{\partial N_4^P}{\partial y} \end{bmatrix}$$

(10)

$$\mathbf{M} = \begin{bmatrix} \dfrac{\partial N_1^u}{\partial x} & \dfrac{\partial N_1^u}{\partial y} & \dots & \dfrac{\partial N_i^u}{\partial x} & \dfrac{\partial N_i^u}{\partial y} & \dots & \dfrac{\partial N_8^u}{\partial x} & \dfrac{\partial N_8^u}{\partial y} \end{bmatrix}; \quad \mathbf{N}^P = \begin{bmatrix} N_1^P & N_2^P & N_3^P & N_4^P \end{bmatrix}$$

Here, N^u refers to the quadratic interpolation function for the displacement field, and N^P refers to the linear interpolation function for the pore pressure field.

The global system of equations is solved by using the trapezoidal rule (Smith and Griffiths 2004).

3. Numerical results

In this Section, we present the results of several numerical simulations. First, we show the influence of the strain-dependent coefficient of permeability on the shape of the consolidation curve on a simple example of a 5 m high embankment resting on a 10 m thick clay layer. Next, we perform numerical simulations of two road embankments: one near the city of Saga, and the other near the city of Boston. Here, we compare computed results against in-situ measurements in order to test and validate our numerical model. All numerical implementations and simulations are performed by

using the finite element code developed by the authors in Fortran.

3.1 5 m high embankment

In this numerical example of a 5 m high embankment resting on a 10 m thick clay layer, we investigate the influence of the strain-dependent coefficient of permeability on the shape of the consolidation curve. The material parameters of the clay are: Young's modulus E=5 000 kPa, Poisson's ratio v=0.2, the initial value of the coefficient of permeability k_0=5·10^{-5} m/day, and the initial void ratio e_0=0.75. The numerical simulations are performed for three different values of the coefficient of the change in permeability α in (Eq. (6)): 0.9 (k1), 1.5 (k2) and 2.5 (k3). The computed results are shown in Fig. 4. We can conclude that the primary consolidation settlements occur at a faster time rate when taking into account the strain-dependency of the coefficient of permeability.
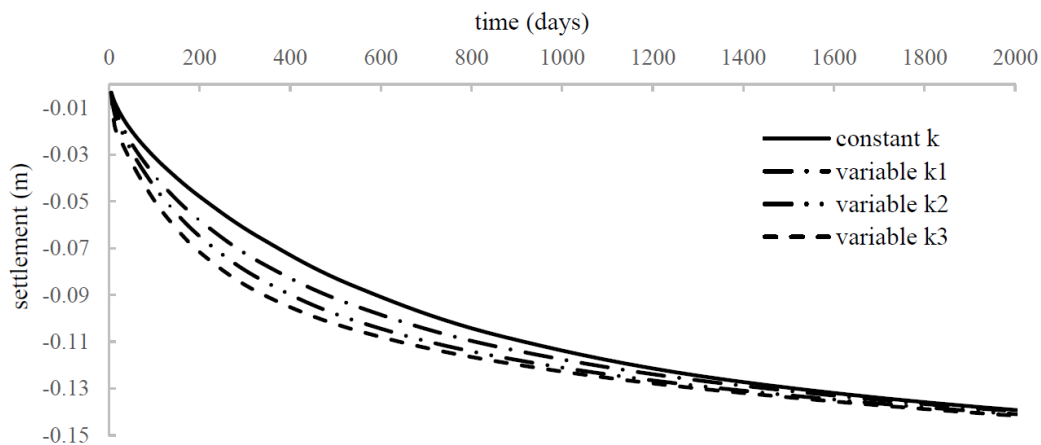

Fig. 4 Computed consolidation curves for the constant and strain-dependent coefficient of permeability

3.2 Road embankment near the city of Saga

The primary consolidation settlement of the road embankment near the city of Saga was numerically analyzed and compared with in-situ measurements by Chai *et al.* (Chai *et al.* 2013). The embankment is 2.5 m high and 13.8 m wide. The embankment slope is 1:1.8. The profile of foundation soil consists of several layers. The behavior of upper layers in (Chai *et al.* 2013). is modeled with the Cam-Clay model (CC), and the behavior of lower layers with a linear elastic model (LE). The foundation soil layers and material properties of interest for our numerical simulations are given in Table 1.

We perform numerical simulations on the numerical model with geometry and boundary conditions shown in Fig. 5. The symmetry of the problem, allows us to analyze only half of the embankment. The width of the numerical model is three times the embankment bottom width. The foundation soil is approximated with four layers. The behavior of all four layers is assumed to be linear elastic. The material properties of layers 3 and 4 are the same as in Table 1. The initial value of the coefficient of permeability for layer 2 is the same as in Table 1, and the initial value of the coefficient of permeability for layer 1 is taken as an average value of coefficients for five upper layers given in Table 1. The values of Young's modulus for layers 1 and 2 are obtained by matching
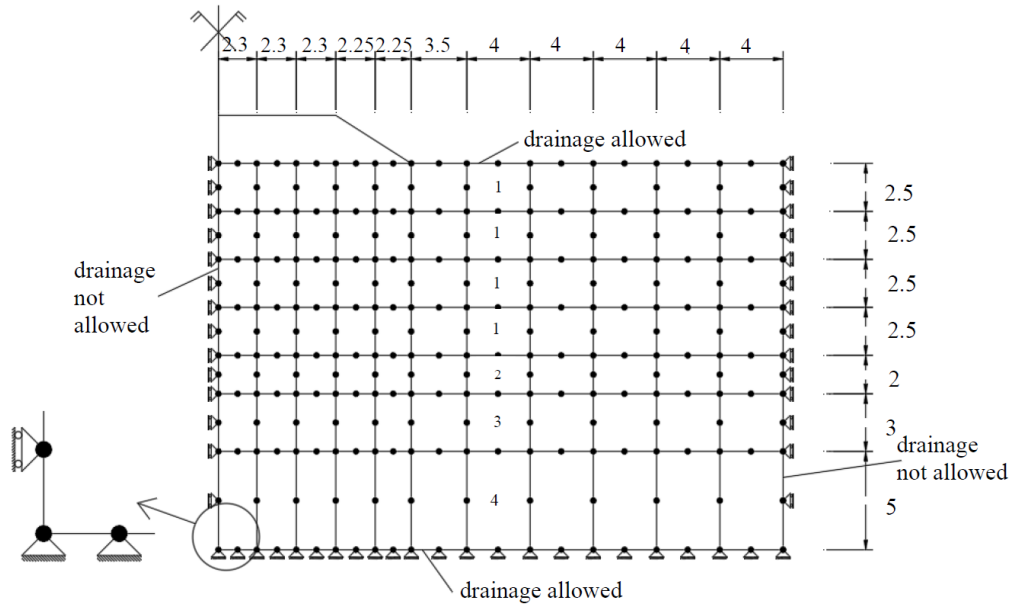
Fig. 5 Numerical model of embankment near the city of Saga

Table 1 Material parameters of foundation soil layers (Chai *et al.* 2013)

Depth	Unit weight γ [kN/m^3]	Young's modulus E [kPa]	Poisson's ratio ν [-]	Initial void ratio e_0 [-]	Coefficient of permeability k_x [10^{-4} m/day]	Coefficient of permeability k_y [10^{-4} m/day]	Constitutive model
0.0-1.5	16.0	-	0.30	1.50	9.1	6.0	CC
1.5-4.0	13.7	-	0.30	3.14	7.7	5.1	CC
4.0-6.0	13.9	-	0.30	2.89	8.1	5.4	CC
6.0-8.0	14.1	-	0.30	2.67	8.1	5.4	CC
8.0-10.0	14.3	-	0.30	2.55	6.9	4.6	CC
10.0-12.0	18.0	-	0.30	1.10	26.3	17.5	CC
12.0-15.0	18.0	20 000	0.25	0.80	2 500	2 500	LE
15.0-20.0	19.0	37 500	0.25	0.70	2 500	2 500	LE

Table 2 Material parameters of foundation soil layers used in numerical model

Layer No.	Depth	Unit weight γ [kN/m^3]	Young's modulus E [kPa]	Poisson's ratio ν [-]	Initial void ratio e_0 [-]	Coefficient of permeability k_x [10^{-4} m/day]	Coefficient of permeability k_y [10^{-4} m/day]
1	0.0-10.0	14.4	235	0.30	2.55	7.95	5.3
2	10.0-12.0	18.0	235	0.30	1.10	26.3	17.5
3	12.0-15.0	18.0	20 000	0.25	0.80	2 500	2 500
4	15.0-20.0	19.0	37 500	0.25	0.70	2 500	2 500

the computed primary consolidation settlement with the measured value. The material parameters of the foundation soil layers used in numerical simulations are shown in Table 2. The coefficient of the change in permeability α in (Eq. (6)) is set to 0.9.
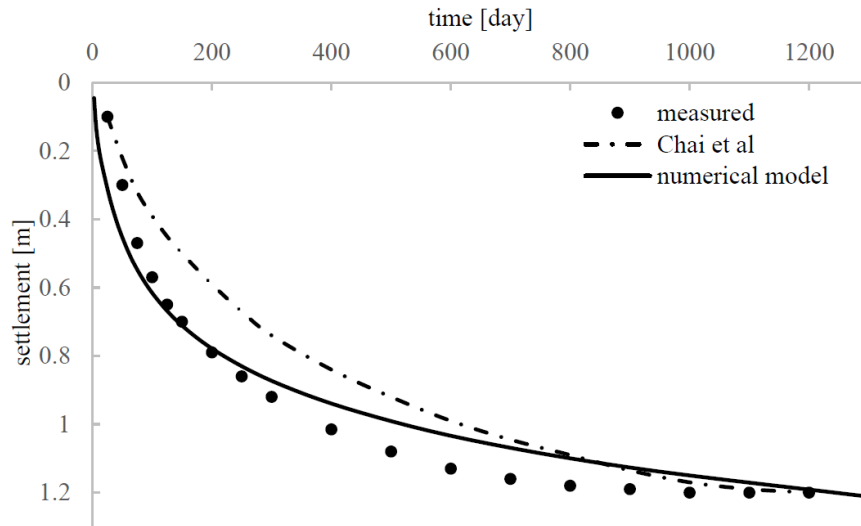
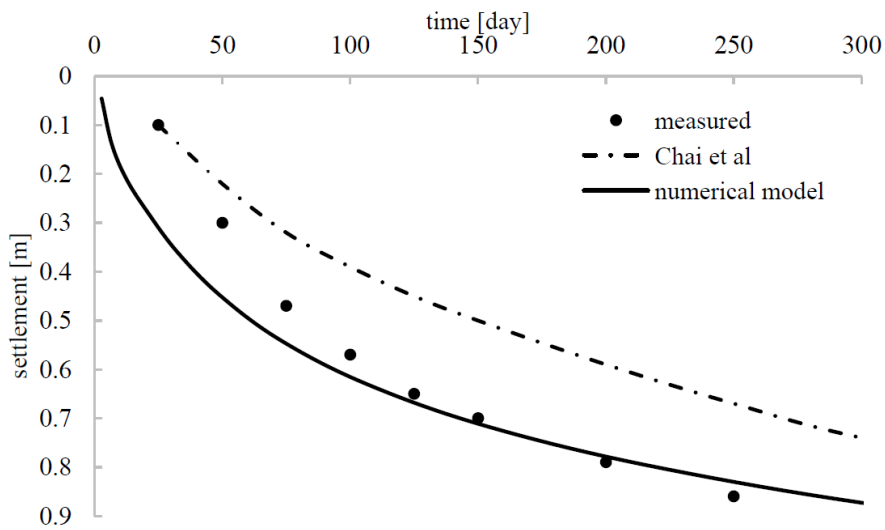Fig. 6 Comparison of consolidation curves

Fig. 7 Comparison of consolidation curves for first 300 days

The computed results are shown in Figs. 6 and 7. We can conclude that a reasonably good match is obtained between the computed results and measured values of settlement, especially for the first 300 days (Fig. 7).

3.3 Road embankment near the city of Boston

The primary consolidation settlement of the road embankment near the city of Boston was numerically analyzed and compared with in-situ measurements by Oliveria and Lemos (2011). The profile of foundation soil consists of three layers. The behavior of the first layer is modeled with a linear elastic model and the behavior of the second and the third layer with elastoplastic models. The
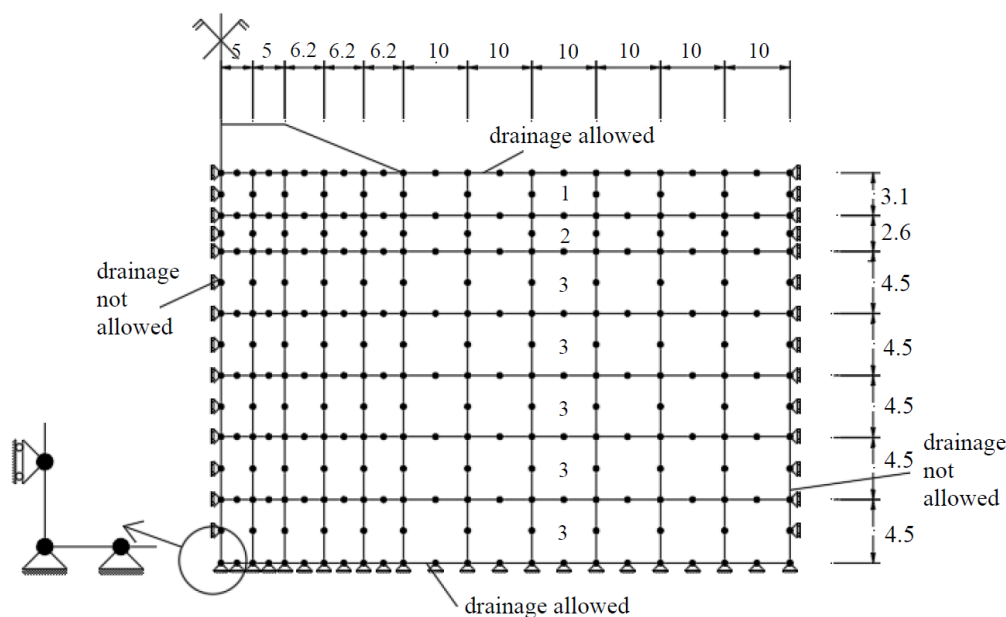
Fig. 8 Numerical model of embankment near the city of Boston

Table 3 Material parameters of foundation soil layers used in numerical simulations

Layer No.	Depth	Unit weight γ [kN/m³]	Young's modulus E [kPa]	Poisson's ratio v [-]	Initial void ratio e_0 [-]	Coefficient of permeability k_x [10^{-4} m/day]	Coefficient of permeability k_y [10^{-4} m/day]
1	0.0-3.1	15.0	10 000	0.30	3.30	10 000	10 000
2	3.1-5.7	15.0	10 000	0.30	3.30	44	11
3	5.7-28.2	15.0	310	0.30	3.30	44	11

geometry and the boundary conditions of the numerical model are shown in Fig. 8.

In our numerical model, we assume the linear elastic behavior of all three layers. The linear elastic parameters of layers 1 and 2 are the same as those used in (Oliveria and Lemos 2011). For layer 3, the coefficient of permeability has the same value as in (Oliveria and Lemos 2011), whereas Young's modulus of elasticity is obtained by matching the computed primary consolidation settlement with the measured value. The material parameters of the foundation soil layers used in numerical simulations are shown in Table 3.

The computed results are shown in Figs. 9 and 10. We can conclude that the computed results do not show a very good match with measured values. The reason for this discrepancy can be explained if we compare the measured consolidation curves for both embankments analyzed with Terzaghi's theoretical consolidation curve (Terzaghi 1943). Terzhaghi's theoretical consolidation curve is obtained from the following expressions

$$s_c(t) = s_c \cdot U_{1/2} \cdot \frac{t}{t_G}; \qquad for\ t \leq t_G$$

$$s_c(t) = s_c \cdot U_{\left(t-\frac{t_G}{2}\right)}; \qquad for\ t > t_G$$
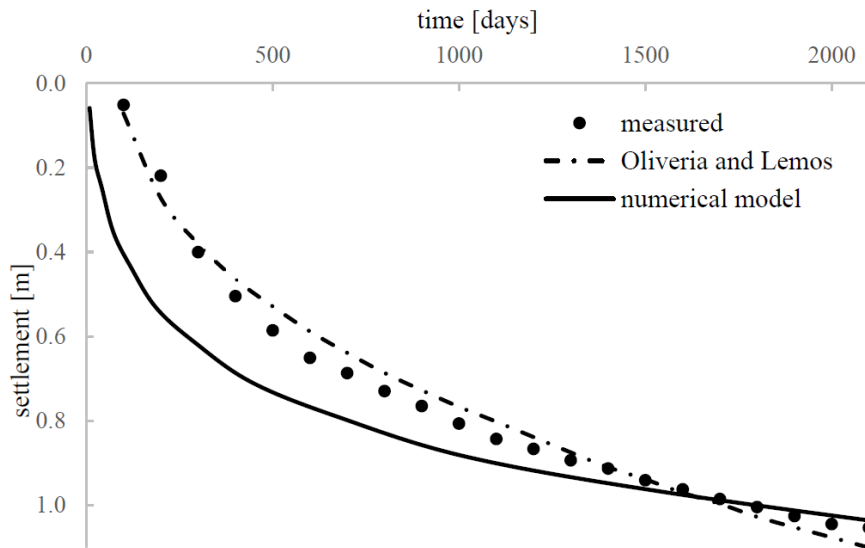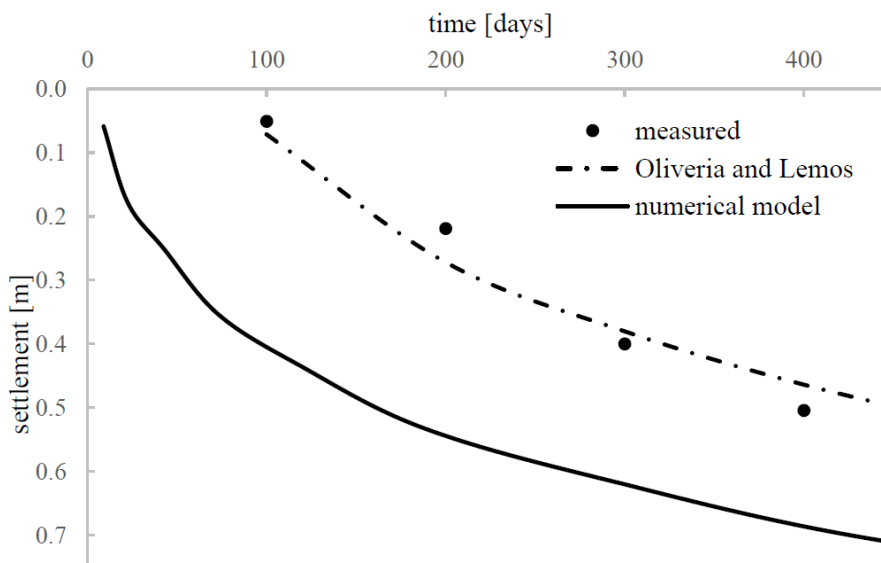
(11)

Fig. 9 Comparison of consolidation curves

Fig. 10 Comparison of consolidation curves for first 450 days

where s_c is the final value of the settlement, $s_c(t)$ is the value of the settlement in time, t_G is the time of load application, and U is the degree of consolidation.

In Fig. 11, the normalized consolidation curves are shown. We can conclude that the measured consolidation curve provided by Chai *et al.* is of similar shape as Terzgahi's theoretical consolidation curve. This is not the case for the measured consolidation curve provided by Oliveria and Lemos, which shows significant deviation from the theoretical one.
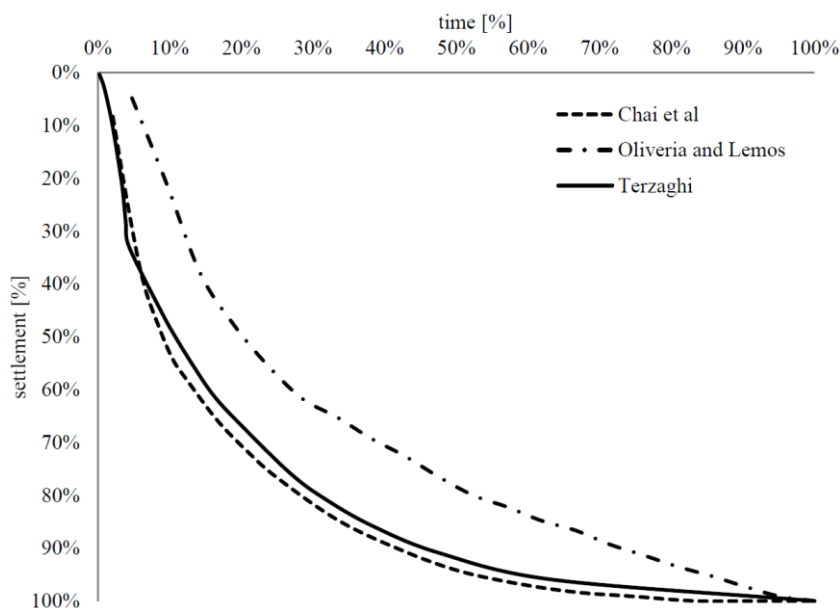
Fig. 11 Comparison of measured consolidation curves with Terzaghi's theoretical consolidation curve

4. Conclusions

In this paper, we have proposed a two-dimensional plane strain numerical model of embankment primary consolidation, which implements Biot's theory of consolidation with both porosity-dependent and strain-dependent coefficient of permeability. First, on a simple example of a 5 m high embankment resting on a 10 m thick clay layer, we have demonstrated the influence of the strain-dependent coefficient of permeability on the shape of the consolidation curve. We have concluded that the faster consolidation time rates are achieved when taking into account the strain-dependency of the coefficient of permeability.

Next, we have performed numerical simulations of two road embankments: one near the city of Saga, and the other near the city of Boston. Here, we have compared computed results against in-situ measurements. A better match of the computed results and in-situ measurements is obtained for the case of embankment near the city of Saga, contrary to the case of the embankment near the city of Boston. To understand why, we have compared the measured consolidation curves against Terzgahi's theoretical consolidation curve. We have concluded that the proposed numerical model gives better results when the measured consolidation curve is of a similar shape as Terzgahi's theoretical consolidation curve.

References

Al-Shakarchi, Y.J., Fattah, M.Y. and Al-Shammary, A.S.J. (2009), "Finite element analysis of embankments on soft clays-Case studies", *J. Eng.*, **15**(1), 3268-3292.
Balic, A. (2018), "Consolidation analysis with deformation-dependent coefficient of soil permeability", doctoral thesis, Faculty of Civil Engineering, University of Sarajevo.

Balic, A., Hadzalic, E. and Dolarevic, S. (2021), "Identification of the strain-dependent coefficient of permeability by combining the results of experimental and numerical oedometer test s with free lateral movement", *Couple. Syst. Mech.*, **11**(1), 1-14. https://doi.org/10.12989/csm.2022.11.1.001.

Biot, M.A. (1941), "General theory of three-dimensional consolidation", *J. Appl. Phys.*, **1941**(12), 155-164. https://doi.org/10.1063/1.1712886.

Chai, J., Igaya, Y., Hino, T. and Carter, J. (2013), "Finite element simulation of an embankment on soft clay-Case study", *Comput Geotech.*, **48**, 117-126. https://doi.org/10.1016/j.compgeo.2012.10.006.

Chin, I.T.Y. (2005), "Embankment over soft clay-design and construction control", *Geotech. Eng.*, **2005**, 1-15.

Di, Y. and Sato, T. (2003), "Liquefaction analysis of saturated soils taking into account variation in porosity and permeability with large deformation", *Comput Geotech.*, **30**(7), 623-635. https://doi.org/10.1016/S0266-352X(03)00060-0.

Geng, X., Xu, C. and Cai, Y. (2006), "Non-linear consolidation analysis of soil with variable compressibility and permeability under cyclic loadings", *Int. J. Numer. Anal. Meth. Geomech.*, **30**, 803-821. https://doi.org/10.1002/nag.505.

Hadzalic, E., Ibrahimbegovic, A. and Dolarevic, S. (2020), "3D thermo-hydro-mechanical coupled discrete beam lattice model of saturated poro-plastic medium", *Couple. Syst. Mech.*, **9**(2), 125-145. https://doi.org/10.12989/csm.2020.9.2.125.

Hadzalic, E., Ibrahimbegovic, A. and Nikolic, M. (2018), "Failure mechanisms in coupled poroplastic medium", *Couple. Syst. Mech.*, **7**(1), 43-59. https://doi.org/10.12989/csm.2018.7.1.043.

Huang, W., Fityus, S., Bishop, D., Smith, D. and Sheng, D. (2006), "Finite-element parametric study of the consolidation behavior of a trial embankment on soft clay", *Int. J. Geomech.*, **6**(5), 328-341. https://doi.org/10.1061/(ASCE)1532-3641(2006)6:5(328).

Ibrahimbegovic, A. (2009), *Nonlinear Solid Mechanics: Theoretical Formulations and Finite Element Solution Methods*, Springer.

Lewis, R.W. and Schrefler, B.A. (1998), *The Finite Element Method in the Static and Dynamic Deformation and Consolidation of Porous Media*, John Wiley and Sons.

Li, C. (2014), "A simplified method for prediction of embankment settlement in clays", *J. Rock Mech. Geotech. Eng.*, **6**(1), 61-66. https://doi.org/10.1016/j.jrmge.2013.12.002.

Liang, F., Song, Z. and Jia, Y. (2017), "Hydro-mechanical behaviors of the threedimensional consolidation of multi-layered soils with compressible constituents", *Ocean Eng.*, **131**, 272-282. https://doi.org/10.1016/j.oceaneng.2017.01.009.

Maksimović, M.M. (2008), *Mehanika tla (eng. Soil Mechanics)*, AGM Knjiga.

Müthing, N., Zhao, C., Hölter, R. and Schanz, T. (2018), "Settlement prediction for an embankment on soft clay", *Comput. Geotech.*, **93**, 87-103. https://doi.org/10.1016/j.compgeo.2017.06.002.

Oliveira, P.J.V. and Lemos, L.J.L. (2011), "Numerical analysis of an embankment on soft soils considering large displacement", *Compute. Geotech.*, **38**(1), 88-93. https://doi.org/10.1016/j.compgeo.2010.08.005.

Plaxis 3D Reference Manual (2021), Bentley.

Radhika, B.P., Krishnamoorthy, A. and Rao, A.U. (2020), "A review on consolidation theories and its application", *Int. J. Geotech. Eng.*, **14**(1), 9-15. https://doi.org/10.1080/19386362.2017.1390899.

Rowe, P.W. (1959), "Measurement of the coefficient of consolidation of lacustrine clay", *Geotechnique*, **9**(3), 107-118. https://doi.org/10.1680/geot.1959.9.3.107.

Singh, M. and Sawant, V.A. (2014), "Parametric study on flexible footing resting on partially saturated soil", *Couple. Syst. Mech.*, **3**(2), 233-245. https://doi.org/10.12989/csm.2014.3.2.233.

Smith, M. and Griffiths, D.V. (2004), *Programming the Finite Element Method*, 4th Edition, John Wiley & Sons.

Tasiopoulou, P., Taiebat, M., Tafazzoli, N. and Jeremic, B. (2015a), "Solution verification procedures for modeling and simulation of fully coupled porous media: static and dynamic behavior", *Couple. Syst. Mech.*, **4**(1), 67-98. https://doi.org/10.12989/csm.2015.4.1.067.

Tasiopoulou, P., Taiebat, M., Tafazzoli, N. and Jeremic, B. (2015b), "On validation of fully coupled behavior of porous media using centrifuge test results", *Couple. Syst. Mech.*, **4**(1), 37-65.

https://doi.org/10.12989/csm.2015.4.1.037.

Terzaghi, K. (1943), *Theoretical Soil Mechanics*, Wiley.

Wong, R.C.K. and Li, Y. (2001), "A deformation-dependent model for permeability changes in oil sand due to shear dilation", *J. Can. Petrol. Technol.,* **40**(08), ETSOC-01-08-03. https://doi.org/10.2118/01-08-03.

Wood, D.M. (2009), *Soil Mechanics: A One-Dimensional Introduction*, Cambridge University Press, New York.

Xie, K.H. and Leo, C.J. (2009), "Analytical solutions of one-dimensional large strain consolidation of saturated and homogeneous clays", *Comput. Geotechnics*, **31**(4), 301-314. https://doi.org/10.1016/j.compgeo.2004.02.006.

Zhuang, Y.C., Xie, K.H. and Li, X.B. (2005), "Nonlinear analysis of consolidation with variable compressibility and permeability", *J. Zhejiang Univ. Sci.*, **6A**(3), 181-187. https://doi.org/10.1007/BF02872317.

Zienkiewicz, O.C. and Taylor, R.L. (2005), *The Finite Element Method*, Vols. I, II, III, Elsevier.

Zou, S.F., Li, J.Z., Wang, Z.J., Lan, L., Wang, W.J. and Xie, X.Y. (2017), "Seepage test and empirical models for soils based on GDS apparatus", *J. Zhejiang Univ. (Eng. Sci.)*, **51**(5), 856-862.